# Welding Characteristics of 5 kW Class $CO_2$ Laser†

Katsunori INOUE*, Junji MIYATA** and Yoshiaki ARATA***

**Abstract**

*The characteristics of 5 kW class $CO_2$ laser beam are investigated, the mode pattern and the forcussing characteristics are measured.*

*The welding characteristics of this beam are investigated experimentally by incorporation of the measured beam characteristics.*

*The problems of the elimination of the metal vapor and the reflection loss of the incident beam are also examined.*

**KEY WORDS:** (Laser Welding) (Equipment) (Mode Pattern) (Focussing) (Bead Parameter) (Metal Vapor) (Reflection)

## 1. Introduction

High power lasers more than several kilo watts are not widely used in Japan at present, therfore, the fundamental characteristics of their heat processing ability and the necessary technique for the research and practical works on the actual heat processings are not know so much. It is necessary for us to have a full knowledge of them when we want to set about the work on the laser heat processings.

From this point of view, the welding characteristics were investigated by using a laser apparatus of 5 kW class output power in this reports.

The results of the measurement of the laser beam profiles such as the mode pattern, the position of the focussing point and the beam diameter at and near by the focussing point in case the beam was converged by a lens system, are shown in the first part of the report.

The bead on plate welding experiments were made under the various conditions and the bead parameters such as the penetration depth and the bead width were measured by incorporation of the previously measured beam profile. These results are shown in the next part.

The influences of the blow off elimination of the metal vapor, which was induced by the laser irradiation, on the weld bead parameters were examined. The measurements of the reflection of the incident laser power were also made. They are shown in the last part.

## 2. Experimental Apparatus

The block diagram of the laser heat processing system used in this study is shown in **Fig. 1**. The laser generator which includes the power system, the laser oscillator and the focussing unit is product of GTE Sylvania (Model 975, at present, a product of Spectra-Physics) in U.S.A.. Maximum output power of this generator is 5.5 kW. The laser beam output from the laser head is bent with the bender mirror by 90 degree, focussed by the lens and heats the objective material to be processed.

Other systems were assembled by Welding Research Institute of Osaka University. The temperature of the cooling water for the laser head is controlled to keep constant in the cooling system so that the laser output power may become stable. The control computer - a microcomputer in the carriage and shutter control system controls the carriage movement and the on-off action of the shutter of the laser head.

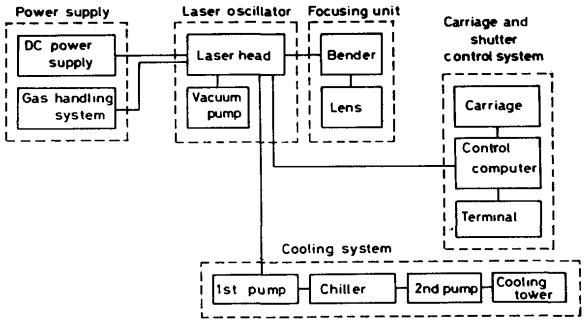


**Fig. 1** Block diagram of experimental apparatus

† Received on October 9, 1981

* Professor

** Graduate student of Osaka Univ. (Presently, Mistubishi Electric Co., Ltd.)

Transactions of JWRI is published by Welding Research Institute of Osaka University, Suita, Osaka, Japan

The photographs of the laser head, the focussing unit and the cooling system are shown in **Fig. 2 (a), (b)** and **(c)**.

## 3. Measurement of Beam Profile

### 3.1 Mode pattern

The mode patterns as the burn patterns on an acryl plate with the different output power are shown in **Fig. 3 (a), (b), (c)** and **(d)**, which were obtained at the input aperture for the beam bender. All of them are of multi-mode and have irregular intensity distribution.

### 3.2. Position of focussing point

The decision of the accurate position of the focussing point was made as follows. The traces of the focussing beam on an acryl resin plate which was set parallel to the beam and was grazed by a half side of the beam was obtained as shown in **Fig. 4 (a)**. The width y along the direction of the depth of the traces x (see Fig. 4 **(b)**) was measured. The measured data were approximated with the following two equations; $y = Ae^{-\alpha x}$, $y = Be^{-\beta x}$, and their intersection was defined as the focussing point. (see **Fig. 4 (c)**) Example of the measurement and the approximation are shown in **Fig. 5**.

The relation of the laser power and thus decided positions of the focussing point was examined on the lenses of three different values of nominal focal length. The result is shown in **Fig. 6**, where the actual focal length becomes shorter as the power increases. It is deduced that this phenomenon is due to the thermal deformation of the lens, caused by the laser absorption.

### 3.3. Beam diameter at and near by focussing point

The cross section of the acryl work-piece engraved by the laser energy is shown in **Fig. 7**. The work-piece was moved at high speed in the perpendicular plane to the laser beam axis at and near by the focussing point. The beam radius and the radial intensity distribution can be got from this engraved workpiece if we assume that all

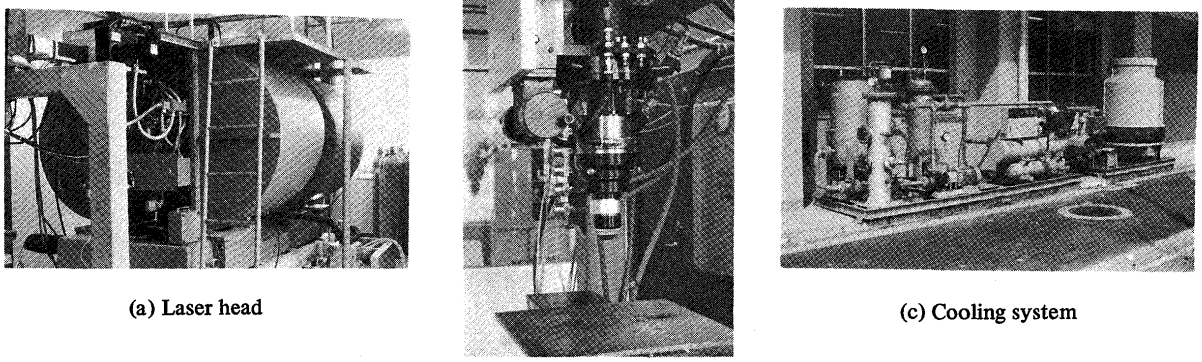

(a) Laser head (b) Focussing unit (c) Cooling system

**Fig. 2** View of laser system

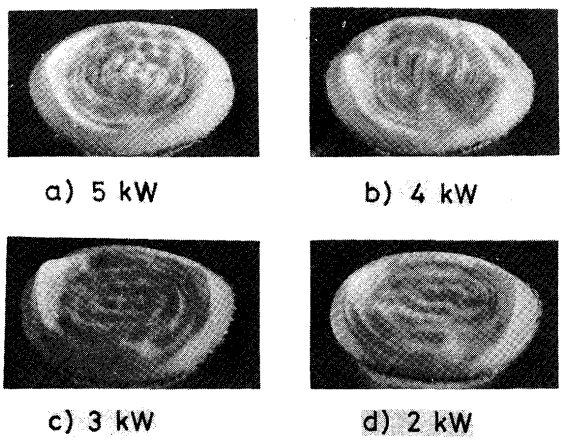


**Fig. 3** Mode patterns at various laser powers

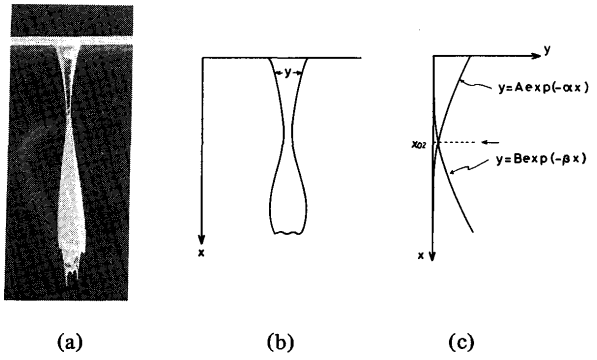


**Fig. 4** Traces of beam locus and its expornential approximation

the laser power is consumed to evaporate and to remove acryl and the depth of the grave is proportional to the power intensity. The removal efficiency $E_r$ is calculated by **Equation (1).**

$$E_r = S\,v\,L/P \times 100\,(\%) \qquad (1)$$

, where S; the removed area in the cross section ($cm^2$) v; the travelling speed of the work piece (cm/sec) L; the latent heat for evaporation of the objective material (the workpiece) p; the laser power (W (= J/sec))

The relation of the travelling speed v and the removal efficiency $E_r$ is shown in **Fig. 8**, L was put to be 3500 ($J/cm^3$) for acryl in this figure. It proves that the efficiency $E_r$ becomes 100% and the intensity distribution profile approaches Gaussian when the travelling speed exceeds the certain limit for the various laser powers as are seen in **Fig. 9 (a)** and **(b)**. The intensity profile was approximated by Gaussian distribution on using a least square method, the experimental beam radius $d_e$ and the Gaussian approximated beam radius $d_a$ were defined as the width at 1/e height of the maximum value in each case respectively.

The relation of the measured beam radius $d_a$ and the laser power for the different focal length lenses is shown in **Fig. 10.** The power density obtainable with these lenses is also shown.

The distribution profile becomes deformed and the beam radius becomes larger as the measured position becomes apart from the focussing point as shown in **Fig. 11 (a)** and **(b).** The broken line in Fig. 11 (b) expresses the simple geometrical beam converging locus.

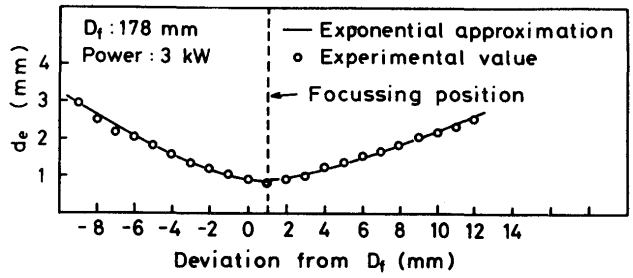


**Fig. 5** Measured value and expornential approximation for beam traces

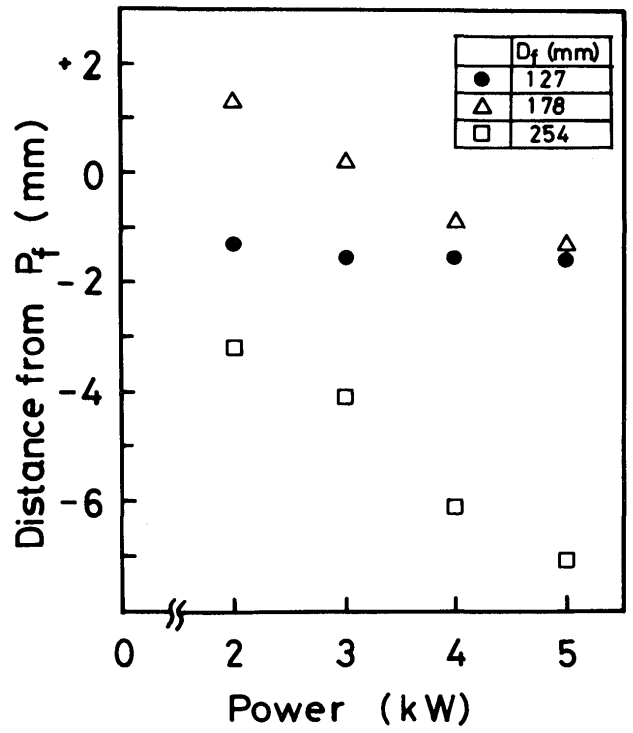


**Fig. 6** Change of focal length of lens by laser power

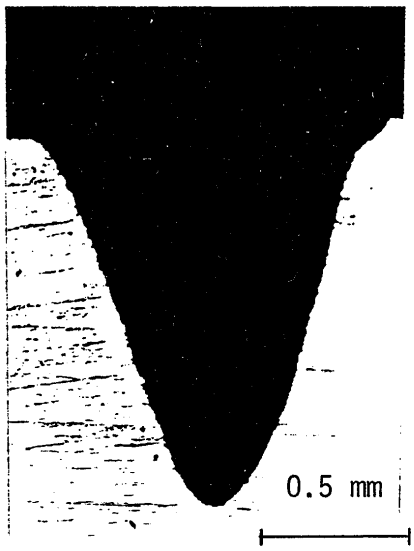


**Fig. 7** Cross section of engraved acryl specimen

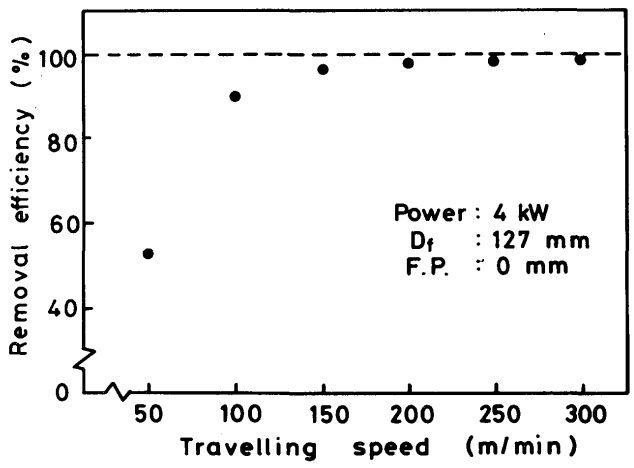


**Fig. 8** Relation of travelling speed and removal efficiency

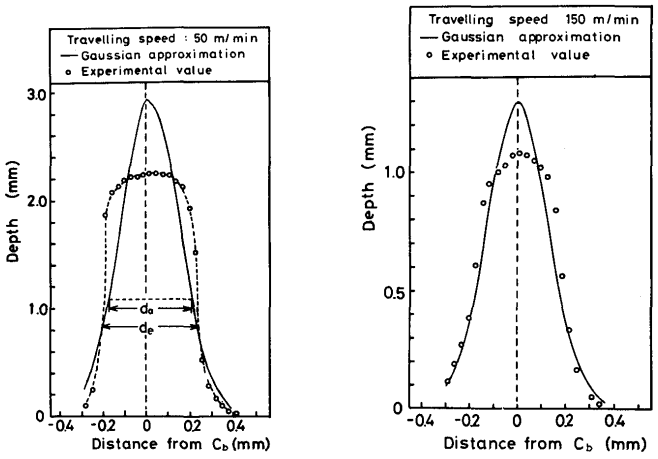


(a) v = 50 (m/min) (b) v = 150 (m/min)

**Fig. 9** Gaussian approximation of beam intensity distribution at focussing point

## 4. Welding Conditions and Bead Parameters

The welding experiments were made on the workpieces of SUS 304 stainless steel and the bead parameters such as the penetration depth and the bead width were measured on the weld cross section. **Figure 12** is the illustration for the experimental arrangement. The X-Y table was used as the carriage for the workpiece. Its motion was controlled with the microcomputer. Argon gas was used as the metal vapor (plasma) blow off gas and the center gas and air was used as the lens protection gas.

### 4.1. Position of focussing point and bead paramenters

The non-dimensional value Id which is the simple geometrical ideal beam diameter and can become the index of the relative position of the focussing point is defined by **Equation (2).**

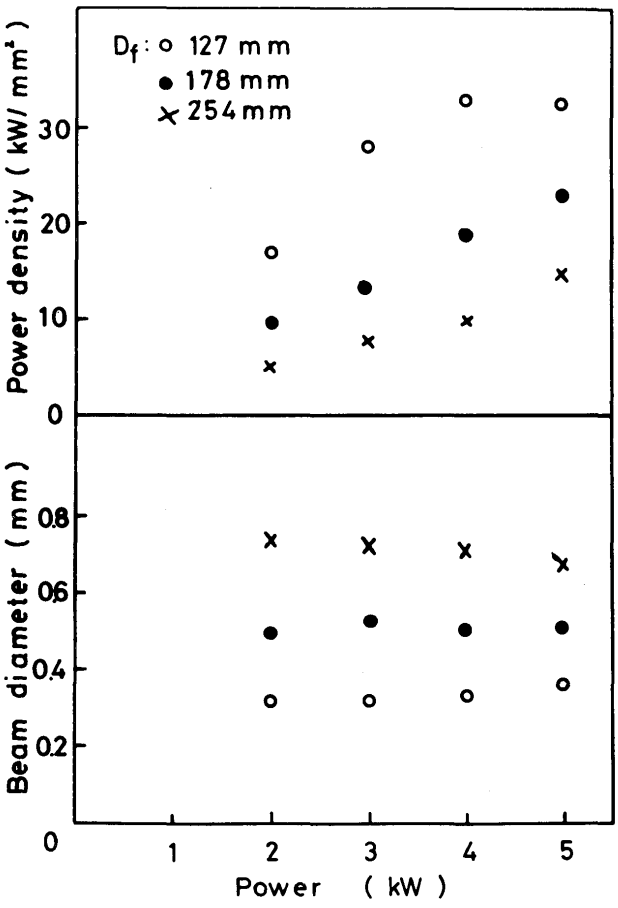


**Fig. 10** Relation of laser power and converged beam diameter, obtainable power density at focussing point

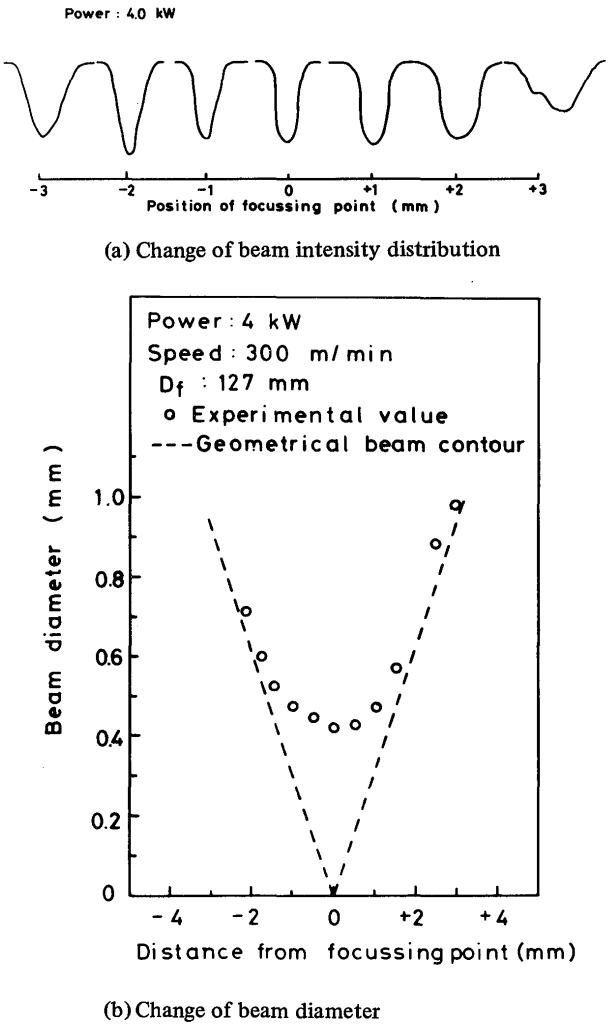


(a) Change of beam intensity distribution

(b) Change of beam diameter

**Fig. 11** Change of beam intensity distribution and beam diameter with relative position of focussing point

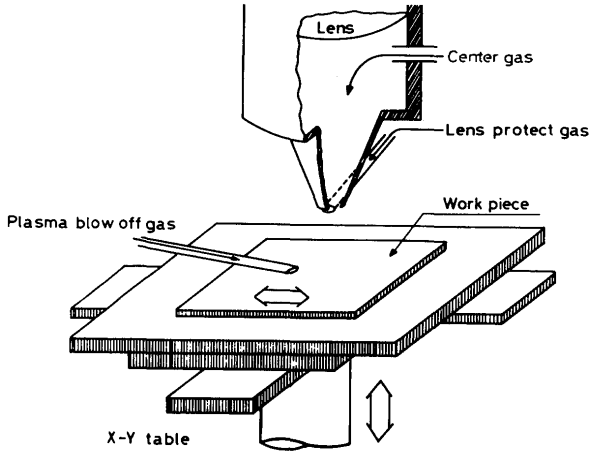


Fig. 12 Illustration for welding experiment

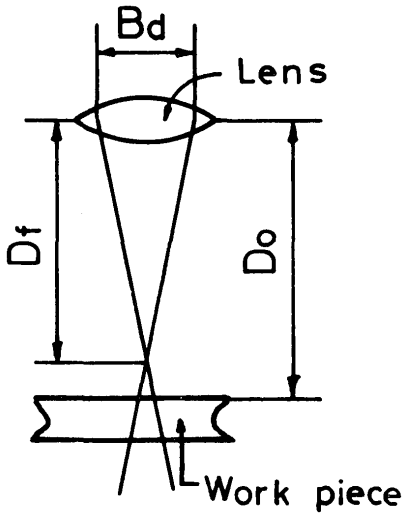


Fig. 13 Definition for $D_f$, $D_o$ and $B_d$

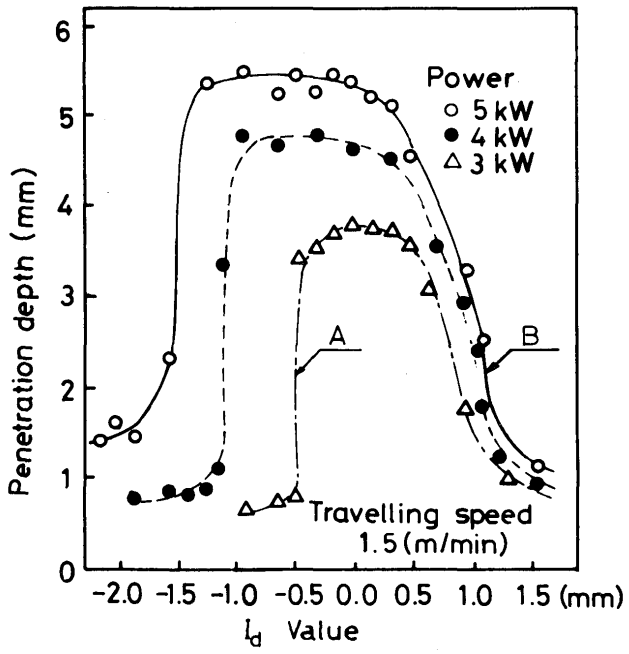


Fig. 14 $I_d$ and $h_p$ : P is parameter

$$I_d = (D_o - D_f) B_d / D_f \quad (2)$$

, where $D_o$, the distance between the lens and the object. (the workpiece) $D_f$; the focal length of the lens. $B_d$; the unconverged beam diameter. They are shown in **Fig. 13.**

The relation of $I_d$ and the penetration depth is shown in **Fig. 14, 15** and **16**, where the laser power, the travelling speed of the workpiece and the focal length of the lens are the parameters respectively.

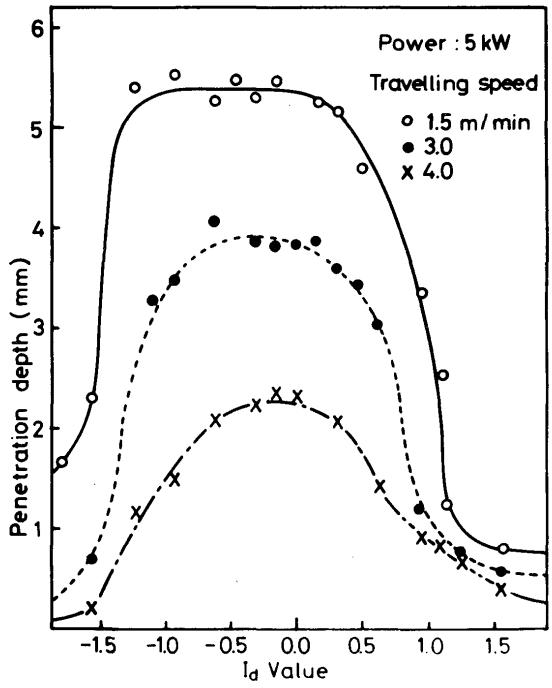


Fig. 15 $I_d$ and $h_p$ : v is parameter

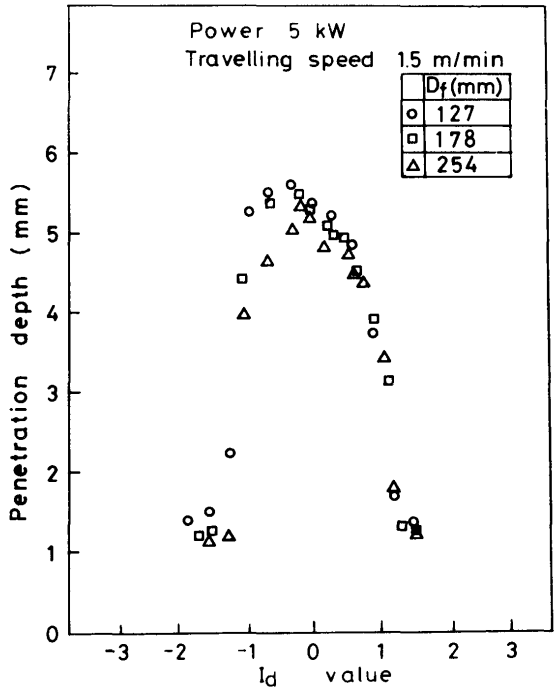


Fig. 16 $I_d$ and $h_o$ : $D_f$ is parameter

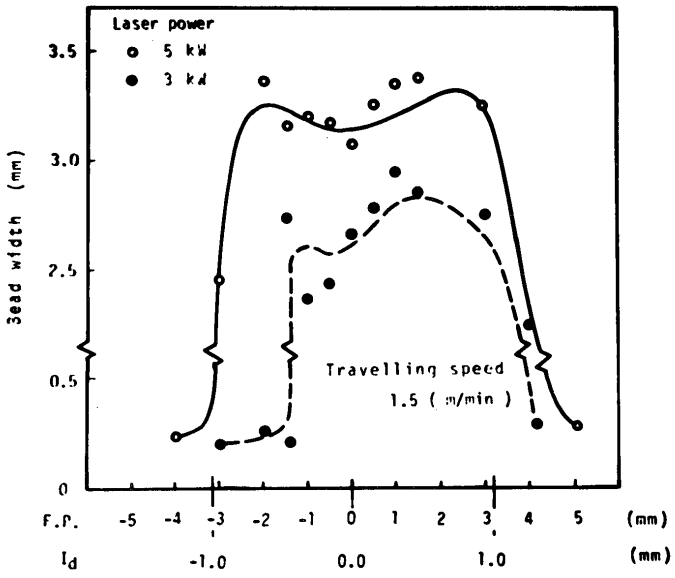


Fig. 17 Relation of $I_d$ and bead width

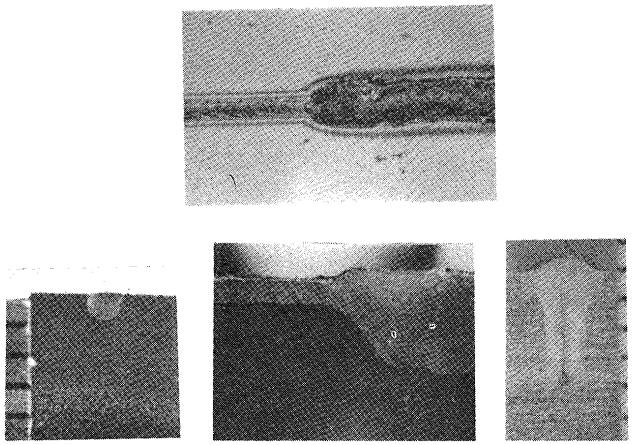

(a) At the point A in Fig. 14

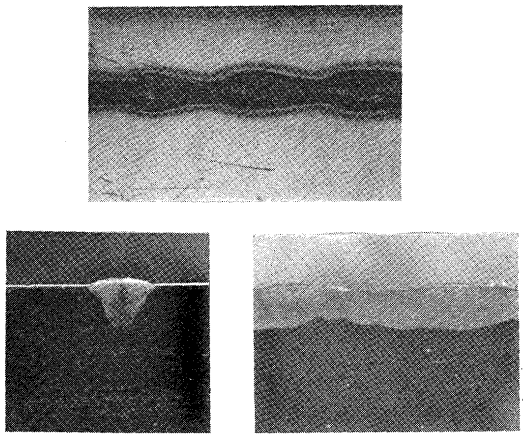

(b) At the point B in Fig. 14

Fig. 18 Bead appearances, cross and longitudinal sections at "the bead transition points"

The relations of $I_d$ and the bead width is shown in Fig. 17.

As are seen in these figures, the bead parameters have the sudden changing points which depends on the value of $I_d$. As the examples, the appearances, the cross and the longitudinal sections at point A and B of Fig. 14 are shown in **Fig. 18 (a)** and **(b)**. The penetration depth and the bead width are changed suddenly and remarkably by the slight change of $I_d$ at the point A and the bead formation becomes unstable at the point B. This phenomenon was named as "the bead transition". The mechanism of the bead transition phenomenon was described in detail in the previous paper[1].

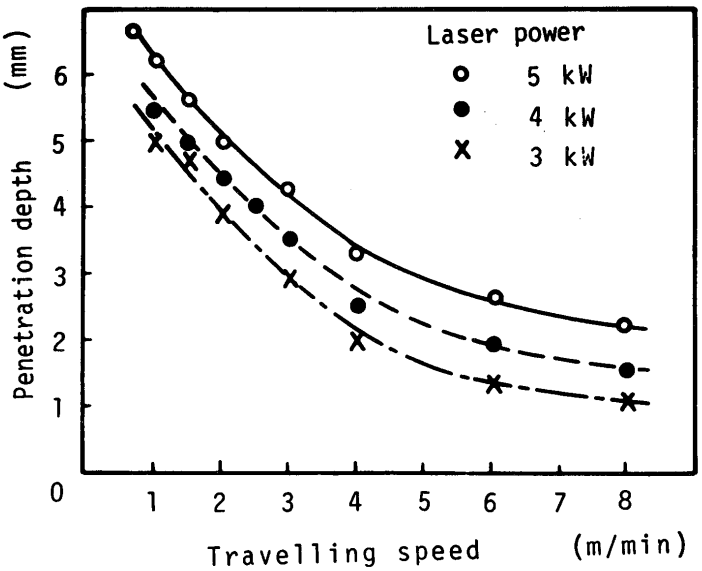


Fig. 19 Relation of travelling speed and penetration depth

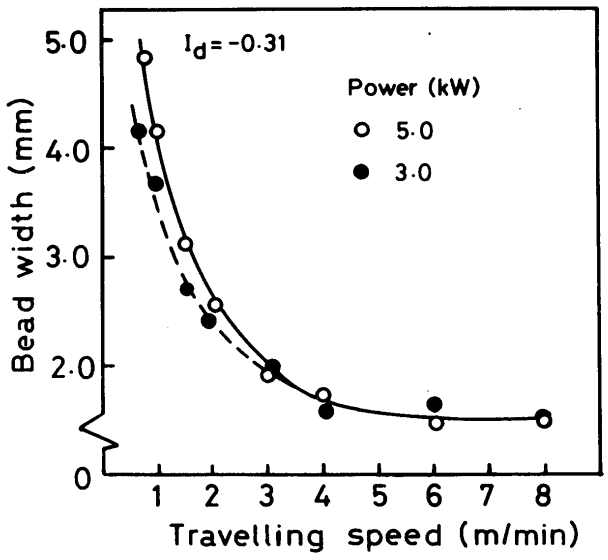


Fig. 20 Relation of travelling speed and bead width

### 4.2. Travelling speed and bead parameters

The relations of the travelling speed and the penetration depth, and the travelling speed and the bead width were shown in **Fig. 19** and **20** respectively. The penetration depth is approximately proportional to −0.6 powers of the travelling speed. The bead width increases steeply for the travelling speed less than 1.5 (m/min).

**Figure 21** shows the bead cross sections for the different travelling speed.

### 4.3. Laser power and bead parameters

**Figures 22** and **23** show the relations of the laser power and the penetration depth, the laser power and the bead width respectively. The penetration depth has a tendency to saturate as the laser power increases.

### 4.4. Consideration based on thermal conduction theory

The non-dimensional values $h_p^*$ and $v^*$ were calculated by substituting the experimental data to the following equation,

$$h_p^* = 8 K T_m h_p / P k$$
$$v^* = v b_w / 4 K_d \qquad (3)$$

where, K; thermal conductivity (0.061 cal/cm sec C°), $T_m$; melting point (1450 C°), $K_d$; thermal diffusivity (0.045 $cm^2$/sec), k; constant of heat equivalent of work (0.239 cal/J) $h_p$; penetration depth, $b_w$; average bead width of the objective material (workpiece) respectively.

**Figure 24** shows the plots of the calculated values on the $v^* - h_p^*$ plane. The solid line in this figure is drawn by the following equation, which is derived from the line heat source approximation of the thermal conduction theory.[2)]

$$h_p^* = 1 / (0.2 + v^*) \qquad (4)$$

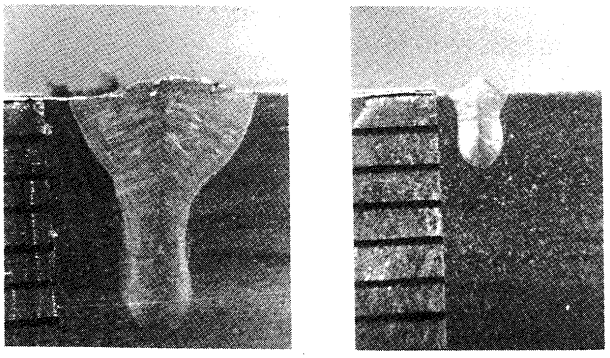

(a) At v = 1.0 (m/min) (b) At v = 8.0 (m/min)

**Fig. 21** Weld cross sections at different travelling speed v

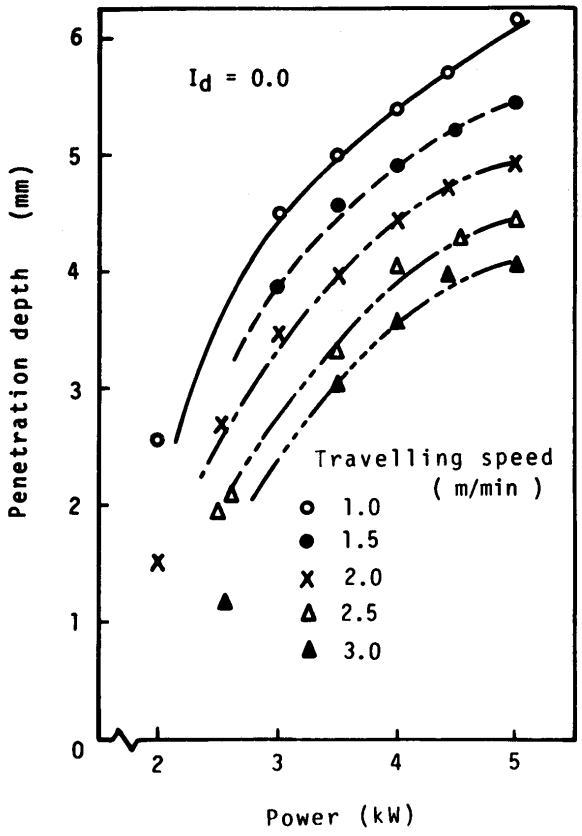


**Fig. 22** Relation of laser power and penetration depth

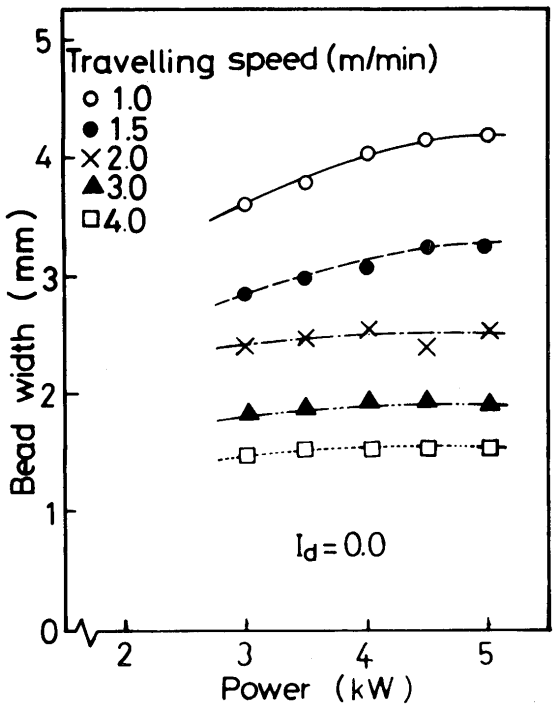


**Fig. 23** Relation of laser power and bead width

The plotted experimental results, from which the data of inadequate $I_d$ value and less power input are excluded, are somewhat different from the theoretical solid line. That difference is based on two reasons. The one is lowering of the joint thermal efficiency, about which the description is made in the next part, due to the reflection loss of the incident laser power. The other is that the actual heat input is different from the line heat source approximation, especialy in case v* is small.

### 4.5. Joint Thermal Efficiency

The ratio of the heat quantity needed to melt the workpiece material of equivalent volume of the weld part to the laser power is defined as "the joint thermal efficiency", which is given in the following equation,

$$E_j = S T_m C_w v / P k \qquad (5)$$

where S; the cross sectional area of the weld part ($cm^2$) $C_w$; the specific heat of the workpiece. Others have been defined.

The relation of the joint thermal efficiency $E_j$ and the ideal diameter $I_d$ is shown in **Fig. 25**. The value of $E_j$ decreases from about 40% to 5% when the bead transition occurs. This difference of $E_j$ is due to the reflection loss.

The relations of $E_j$ and the travelling speed, $E_j$ and the laser power are shown in **Fig. 26** and **27**.

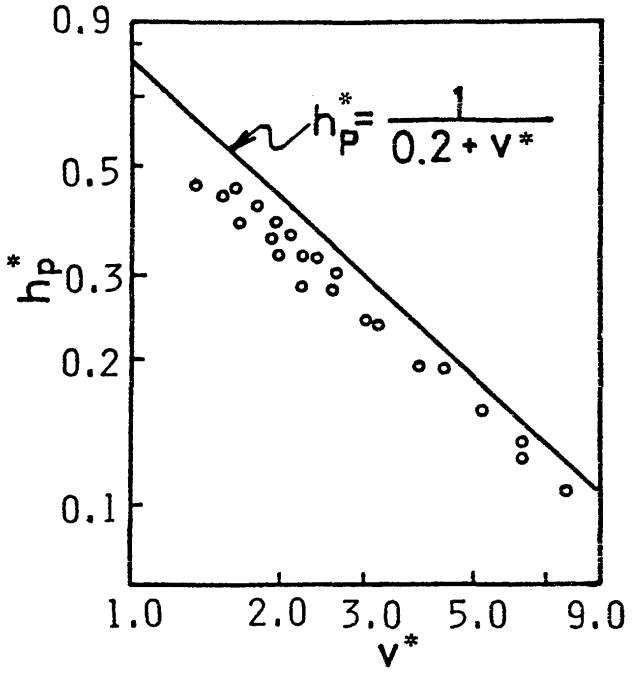


Fig. 24 Relation of v* and $h_p$*

### 5. Elimination of Metal Vapor

It was reported that the metal vapor, generated by the laser heating, from the workpiece disturbs the incident laser power and prevents the proper bead formation,[3] therefore, it should be eliminated. The gas flow was used for this purpose. The arrangement is shown in **Fig. 28**. The shape of the gas nozzle is divergent type and its exit diameter is 0.7 (mm).

The appearances of the metal vapor in case the nozzle clearance C changes are shown in **Fig. 29 (a), (b)** and **(c)**. The luminosity decreases as C decreases, but the penetration depth is not affected by C as shown in **Fig. 30**.

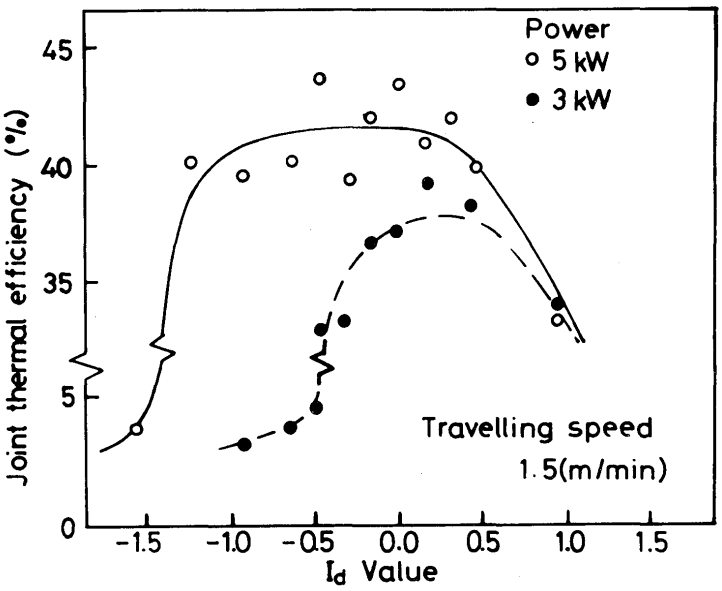


Fig. 25 Relation of $I_d$ and joint thermal efficiency

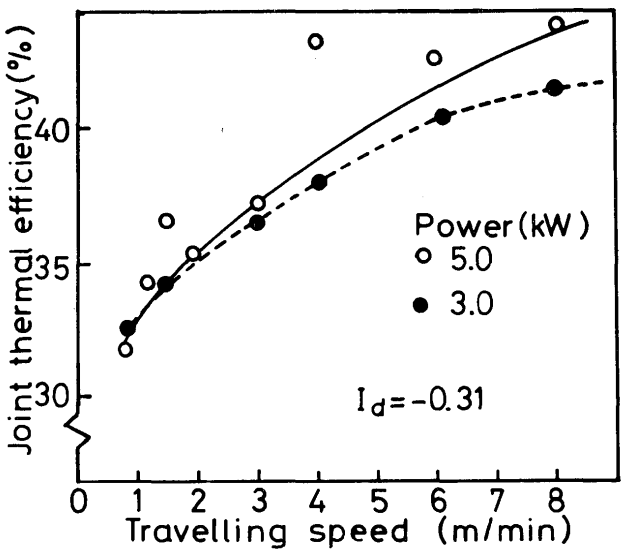


Fig. 26 Relation of travelling speed and joint thermal efficiency

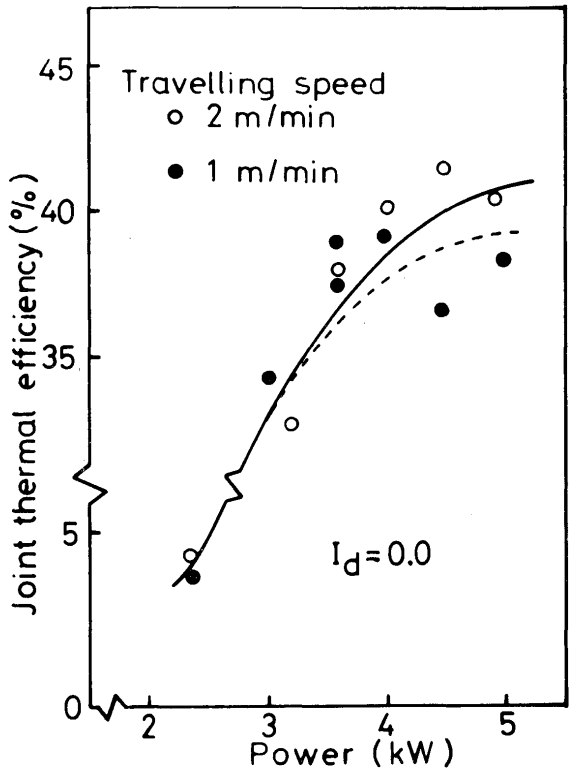


Fig. 27 Relation of laser power and joint thermal efficiency

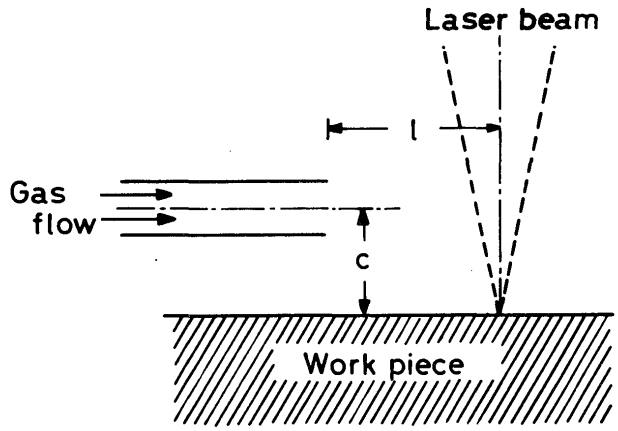


Fig. 28 Schematic of metal vapor blow off arrangement

The luminosity also decreases as the gas flow rate through the nozzle increases, however, also in this case, the bead parameters do not show remarkable change as is seen in **Fig. 31**. The penetration depth decreases slightly if the center gas (see Fig. 12) pressure decreases as shown in **Fig. 32**.

The elimination of the metal vapor by the gas flow has not so notable effect within the region of our experiment.

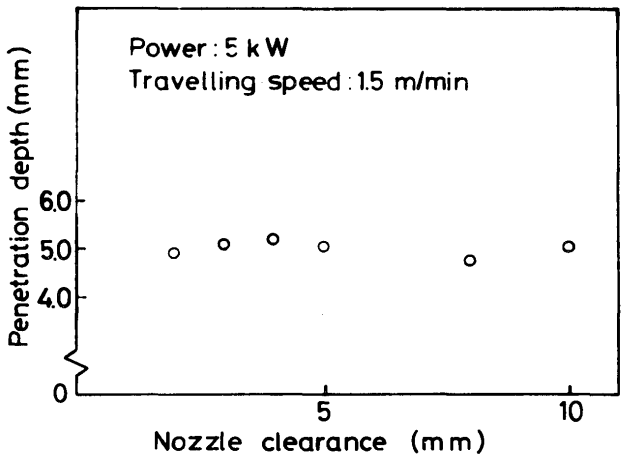


Fig. 30 Relation of nozzle clearance and penetration depth

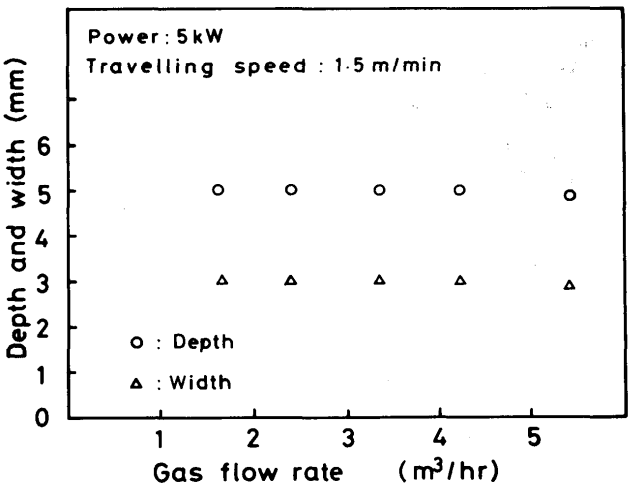


Fig. 31 Relation of gas flow rate for metal vapor elimination and penetration depth, bead width

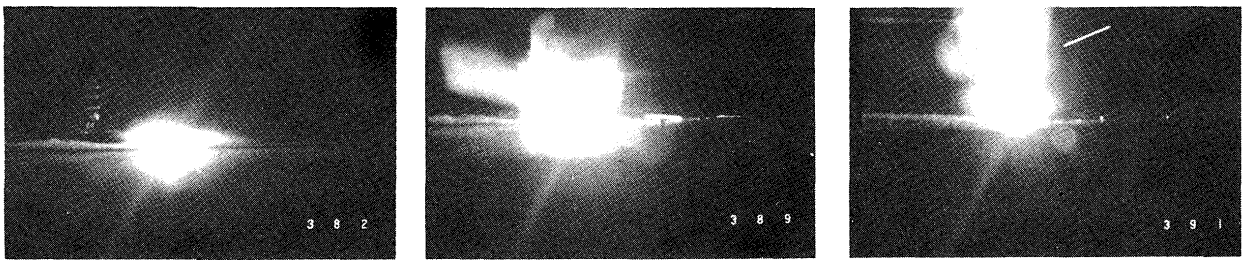

(a) C = 2 (mm) (b) C = 5 (mm) (c) C = 10 (mm)

Fig. 29 Blow off configuration of metal vapor

## 6. Measurement of Laser Power Reflection

The schematic arrangement to measure the laser power reflection is shown in **Fig. 33**. The reflected laser power from the workpiece heats, evaporates and removes the surface of the acryl plate which is supported parallel to the worpiece. **Figure 34** shows the typical acryl specimen whose surface was removed by the laser reflection. The hole at the center is the nozzle aperture for the beam, the unremoved part at the lower side is the shade of the nozzle for the lens protection gas flow. The welding direction is from right to left. Correction by which the shade of the nozzle was rejected and the removed part became symmetrical was made. The removed depth, accordingly, the reflected power at the center hole part was assumed to be equal to its surroundings though much more removal was estimated at that part, because the reflection power to the incident direction must be maximum. The integral reflected power was calculated from the volume of the corrected removed part by using the similiar equation as Equation (1). Errors due to many factors such as the underestimation for the reflection at the center hole, the power loss at the acryl evaporation, the radiation heating from the workpiece and the metal vapor and etc. were neglected in the calculation. The integral reflected power was converted into the reflected power per unit length of the weld line.

**Figure 35** shows the relations among the travelling speed, the reflected power and the ratio of the reflected to the incident power. The reflected power per unit weld length is kept constant as the travelling speed changes, therefore, the ratio of the reflected to the incident is proportional to the travelling speed. It is seemed to be contrary to the fact shown in Fig. 26, where the joint thermal efficiency increases as the travelling speed increases. In Fig. 35, the reflecting ratio becomes about 15% when the travelling speed is 6 (m/min). The joint thermal efficiency is over 40% as is seen in Fig. 26 under the same condition, so the melting efficiency becomes about 50%, which is almost equivalent to the value derived from the line heat source approximation of the thermal conduction theory.[2] The measured reflecting ratio is much lower at the lower travelling speed than at the higher travelling speed, but the joint thermal efficiency is lower in the former case. It can be explained as follows. Generation of the metal vapor is more at the lower travelling speed and the incident laser is more apt to be absorbed and scattered by that vapor. Such power loss can not be sensed by the acryl evaporating method adopted in this work.

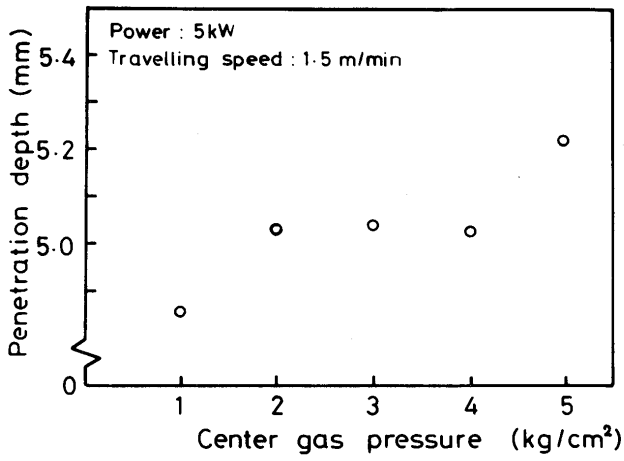


**Fig. 32** Relation of center gas pressure for lens protection and penetration depth

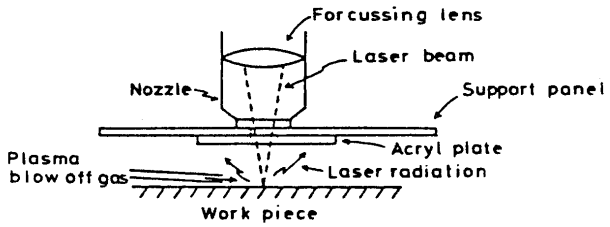


**Fig. 33** Schematic of laser power reflection measurement

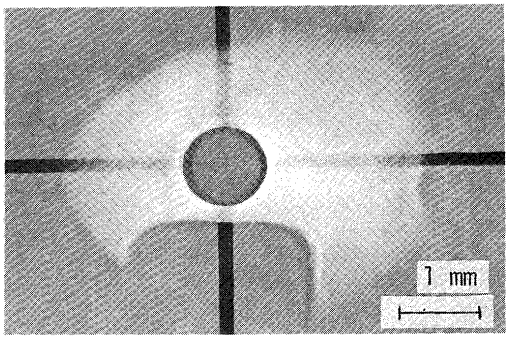


**Fig. 34** Example of acryl specimen whose surface was removed by laser reflection

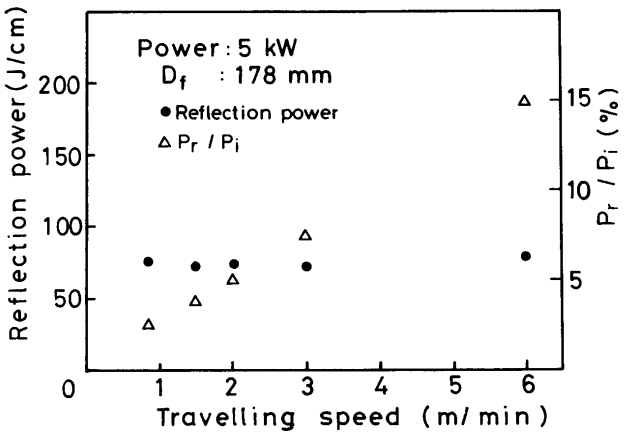


**Fig. 35** Relations among travelling speed, reflected power per unit weld length and ratio of reflected power to incident power

## 7. Conclusion

This report is summarized as follows.

1) The focal length of the ZnSe lens which is on the market at present changes by several milli-meter as the laser power changes. The changing amount of focal length with power depends on the nominal focal length of the lens itself. The longer the focal length is, the larger the changing amount becomes.
2) The spot diameter of the converging laser beam at the focussing point is several tenth milli-meter. It also becomes somewhat larger as the focal length of the lens increases. The power density obtainable with the lens depends on its focal length as the result.
3) The $I_d$ value is defined as the index of the relative position of the focussing point. The proper penetration can be obtained within the certain region of the $I_d$ value. The bead transition phenomenon occurs suddenly if the $I_d$ value deviates from that region. The workpiece is hardly melted under this condition.
4) The penetration depth has saturating tendency with the laser power and is proportional to $-0.6$ powers of the travelling speed.
5) The experimental results agree well with the theoretical within the certain difference. It is presumed that this difference is mainly due to the power loss such as reflection, scatter and absorption of the incident beam by the workpiece and the metal vapor.
6) Errors due to various causes can not be neglected in the power reflection measurement by acryl evaporating method. It is necessary to perform more precise measurement to back up the result of the measurement made in this report.

### Acknowledgement

The authors wish to express appreciation to Spectra Physics in U.S.A. and Marubun Co. in Japan for providing some materials necessary for the experiment and also to Mr. S. Matsumura, Mr. K. Fukiwake, Mr. T. Mitsumune, and Mr. K. Mori for their cooperations to this work.

### References

1) Y. Arata, K. Inoue, H. Maruo and H. Miyamoto, Characteristics of High Power $CO_2$ Laser Welding, Beam Technology, Deutscher Verband für Schweißtechnik (1980).
2) A.A. Wells, Heat Flow in Welding, Welding Journal, Vol. 31 (1952), No. 5, 263s-267s.
3) E.V. Locke, E.D. Hoag and R.H. Hella, Deep Penetration Welding with High-Power $CO_2$ Lasers, IEEE Journal of Quantum Electronics, Vol. qe-8 (1972), No. 2, 132-135.